Macromolecules

Article

pubs.acs.org/Macromolecules

Self-Assembly of Ionizable "Clicked" P3HT-*b*-PMMA Copolymers: Ionic Bonding Group/Counterion Effects on Morphology

Eunkyung Ji,[†] Virginie Pellerin,[†] Laurent Rubatat,[†] Eric Grelet,[‡] Antoine Bousquet,[†] and Laurent Billon*[,†]

[†]IPREM CNRS-UMR 5254, Equipe de Physique et Chimie des Polymères, Université de Pau et des Pays de l'Adour, Hélioparc, 2 avenue Président Angot, 64053 Pau Cedex 9, France and

[‡]CNRS, Centre de Recherche Paul-Pascal, Université de Bordeaux, 115 Avenue Schweitzer, 33600 Pessac, France

Supporting Information

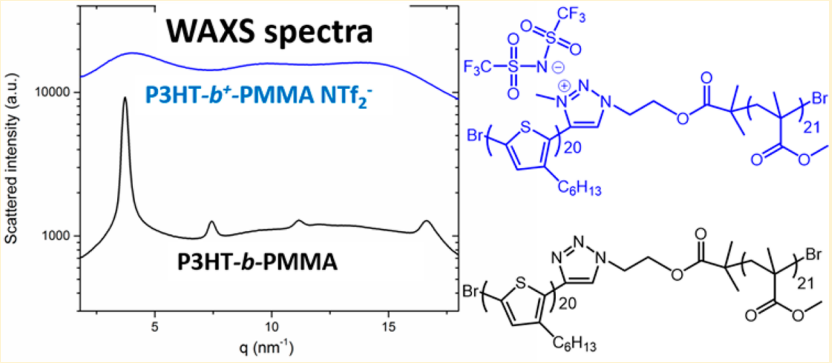

ABSTRACT: A novel methodology used to overcome the predominance of $\pi-\pi$ interactions on the organization of rod−coil copolymer is reported in this paper. We demonstrated changes in the self-assembly morphology of poly(3-hexylthiophene)-*b*-poly(methyl methacrylate) (P3HT-*b*-PMMA) block copolymer BCP, by introducing an ionic group to the linking unit between the two blocks. A neutral polymer precursor was synthesized from ethynyl-terminated P3HT and azido-terminated PMMA via Huisgen's 1,3-dipolar cycloaddition. Then two 1,2,3-triazolium-based block copolymers with different counteranions were obtained by a quaternization of 1,2,3-triazole groups with methyl iodide, and subsequent anion exchange was observed with a fluorinated salt, bis(trifluoromethane) sulfonimide salt. Atomic force microscopy, modulated differential scanning calorimetry, and X-ray scattering were used to prove that the crystallization of the conjugated block is disrupted by the additional ionic interactions imposed to the system. The 1,2,3-triazolium-based BCP with iodide as the counterion exhibited highly organized well-defined fibrils, as the diblock phase segregation χ becomes predominant over the rod−rod interaction μ. When the more stable and larger NTf_2^- was used as counterion, P3HT phase was disrupted and no crystallization was observed. This methodology could be a useful strategy to open the range of nanomorphologies reachable with a semiconducting polymer for electronic or photovoltaic applications.

INTRODUCTION

The block copolymers (BCPs) have gained significant attention due to their ability to self-assemble into a variety of ordered nanostructures; this nanoscale structures enable their use in advanced nanotechnology applications such as electronics, membranes, or batteries.[1−3] The ability of BCP to form nanostructures offers a low-cost nanolithography technique for generating fine patterns. Meanwhile, there has been a growing interest in the synthesis of block copolymers containing conjugated polymers since it may offer a new strategy for the precise and controlled organization of semiconducting polymers. For example, in organic electronic applications, the domain sizes need to be about 10 nm to match the exciton diffusion length, resulting in enhanced optical and electronic properties.[4]

Conjugated polymer are rod macromolecules whose chain rigidity mainly originates from the aromatic monomer unit and the conjugation. A number of theoretical studies have demonstrated that a rod−coil diblock copolymer exhibits a complex self-assembly behavior which is distinctly different from that of conventional coil−coil block copolymer.[5,6] In principle, the final morphology of coil−coil BCPs is determined by the volume fraction f of each block and the product χN where χ is the Flory−Huggins interaction parameter and N is the total degree of polymerization of the copolymer.[7,8] However, in rod−coil BCPs, three additional parameters are required: the Maier−Saupe ($\pi-\pi$) interaction parameter (μ),

Received: September 26, 2016
Revised: November 17, 2016
Published: December 20, 2016

DOI: 10.1021/acs.macromol.6b02101
Macromolecules 2017, 50, 235−243

Scheme 1. Structures of Diblock Copolymers Synthesized in This Study

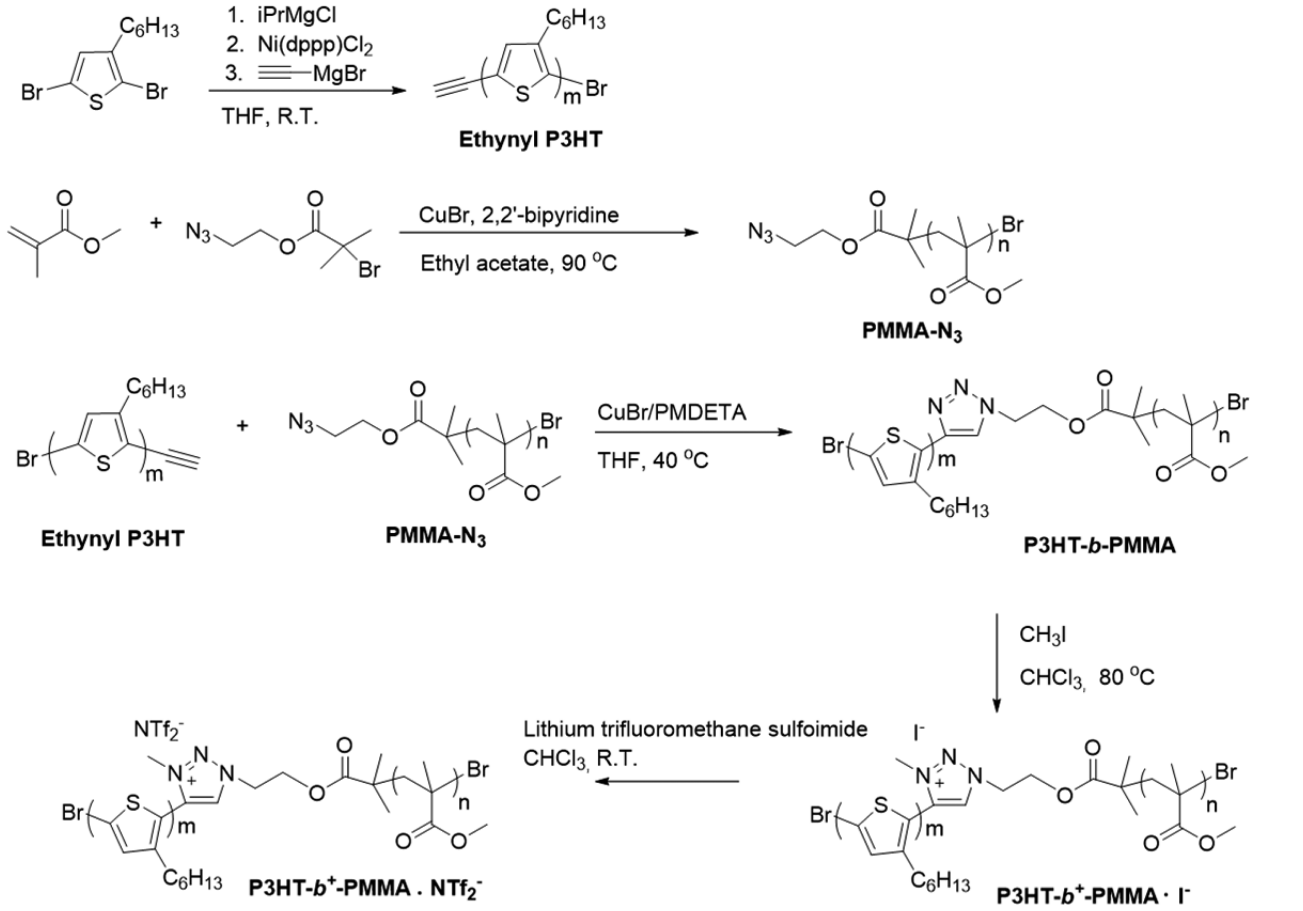

the competition between μ and χ ($G = \mu/\chi$), and geometric asymmetry parameter (rod to coil length ratio, ν).[7,9] In the strong rod−rod interaction regime ($\mu > \chi$), the organization is dominated by the rod crystallization and nanofibrils are obtained as a thermodynamically stable structure. Poly(3-hexylthiophene) (P3HT) block copolymers usually self-organize into these fibrils with a lack of 3D and long-range order, which is a clear problem for lithography.[10−12]

Few strategies have been followed to reduce the predominance of $\pi-\pi$ interaction. Lee et al. studied rod−coil P3HT-*b*-P2VP copolymers in which they varied the coil block size. For coil fractions below 68% they observed fibrils or lamellae morphologies dictated by the rod−rod interactions. For higher coil fractions, the authors showed the change to cylindrical and even spherical phases along with a decrease in crystallization. The authors attributed this behavior to a poor P3HT rods packing resulting from a chain twist generated by the long coil size.[13]

Lin et al. chose to vary the side chain of poly(3-alkylthiophene) (P3AT) block from hexyl to longer dodecyl and to branched 2-ethylhexyl in a diblock copolymer P3AT-*b*-PMMA (poly(methyl methacrylate)).[14] In P3HT-*b*-PMMA the rod−rod interaction is strong and the crystallization of the rod block drives the morphology toward lamellar but most of the time fibril-like structure.[15,16] The introduction of the branched side chain leaded to conformational asymmetry between the P3AT and PMMA segments, to reduce μ value and crystallization driving force. As a consequence hexagonal cylindrical phase was observed for a P3AT fraction of 0.52. Segalman et al. previously studied the impact of the alkyl chains of homo P3AT and showed an important decrease of the melting temperature from 224 °C for the hexyl to 71 °C for the ethylhexyl along with a strong reduction of the Maier−Saupe parameter.[17]

Both strategies leaded to an increase in the influence of χ over μ onto the self-assembly of the diblock copolymer mandatory to reach high-ordered film and diverse morphology; but they present disadvantages. The first path of Lin et al. increase the degree of polymerization of the coil block and therefore the sizes of the domains; in the race to reach patterning under 10 nm, this is not appropriate. The second route from Lin and co-workers change the nature of the conjugated block which will affect the absorption, hole mobility and all the P3HT intrinsic properties, important for organic electronic applications.[18]

We describe a third route to reduce μ influence over χ in order to improve the organization of diblock copolymers containing a semicrystalline block. P3HT block copolymer self-assembly is influenced in this report by introducing ionic functional groups into the polymer chains. Lodge et al. have shown that adding lithium salt to a ternary blend of polystyrene (PS), poly(ethylene oxide) (PEO) and PS-*b*-PEO, dramatically increased the segregation strength of the blend.[19] Ionomers are polymers containing a small number of ionic groups in their hydrophobic backbone.[20] The ionic groups within ionomers can form aggregates of several ionic pairs, called "multiplets" due to the Coulombic interaction (dipole−dipole interaction) between ions embedded in a low dielectric constant matrix.[21]

DOI: 10.1021/acs.macromol.6b02101
Macromolecules 2017, 50, 235−243

Schadler et al. have previously shown that the lamellar spacing of a symmetric poly(styrene-*block*-isoprene) (PS-*b*-PI) BCPs can be tuned by introducing ionic groups at one or both chain ends.[22] The competition between block segregation and ionic aggregation leaded to the observed changes. Following this study, Schops et al. used this principle in a PS-*b*-PI bearing one ionic group at the block junction point and another one with opposite charge at one chain end. They observed a beautiful morphological transition from hexagonally packed cylinders when the ionomer was cast without additive counterion LiCl, to lamellar structures with the addition of LiCl salt.[23] More recently, Hawker et al. reported that an ionic junction in a polydimethylsiloxane-*block*-poly(ethylene oxide) PDMS-*b*-POE leaded to enhanced segregation strength and phase separation due to the electrostatic interactions when compared to the neutral copolymer.[24]

Herein, we report the synthesis of a 1,2,3-triazole "clicked" poly(3-hexylthiophene-*b*-methyl methacrylate) (P3HT-*b*-PMMA) BCP by using Grignard metathesis polymerization (GRIM), atom transfer radical polymerization (ATRP), and Huisgen cyclo-addition, affording the BCP with desired composition, molecular weight, and architecture (Scheme 1).[25] Additionally, two 1,2,3-triazolium-linked BCPs were prepared via quaternization of the 1,2,3- triazole units with methyl iodide and subsequent anion exchange to replace the iodide anion with the more stable bis(trifluoromethane) sulfonimide anion (NTf_2^-).[26] The morphologies of thin films and phase transformations of these BCPs were studied by atomic force microscopy (AFM), modulated differential scanning calorimetry and X-ray scattering to investigate the effect of the ionic group and the counterion on the self-assembly of BCPs.

EXPERIMENTAL SECTION

Materials. All chemicals were purchased from Sigma-Aldrich and used without further purification except copper bromide, methyl methacrylate (MMA) and THF. CuBr was purified by stirring with acetic acid overnight and washing with acetic acid, absolute ethanol, and diethyl ether and then dried in a vacuum oven. MMA was stirred with inhibitor remover for 30 min and filtered. Distilled THF was dried over 3 Å molecular sieve (20% mass/volume) for more than 48 h prior to use.

Characterization. ^{1}H and diffusion order spectroscopy (DOSY) NMR experiments were carried out on a Bruker 400 MHz spectrometer. The molecular weight and molecular weight distribution of all synthesized polymers were measured using size exclusion chromatography (SEC) and THF as eluent (flow rate 1.0 mL min^{-1}) at 30 °C. SEC is equipped with a Viscotek VE 5200 automatic injector, a precolumn and two columns (Styragels HR 5E and 4E (7.8 ft, 300 mm)) and 4 detectors: UV−visible spectrophotometer(Viscotek VE 3210), a Multiangle Light Scattering detector (Wyatt Heleos II), a viscosimeter (Wyatt Viscostar II) and a refractive index detector (Viscotek VE 3580). Polystyrene standards were used to determine the dispersity of the polymers. Fourier transform infrared (FTIR) spectra were collected on a Nicolet Magna in a reflectance mode. All FTIR samples were prepared as a powder with KBr (93 wt %). Atomic force microscopic (AFM) images were obtained using MultiMode 8 Atomic Force Microscope (AFM) from Bruker in a PeakForce QNM (Quantitative NanoMechanics) mode. The polymers samples were prepared by spin-coating from toluene solution (10 mg/mL) onto silicon wafers, followed by thermal annealing (80 °C for 1 h and 200 °C for 10 min).

Differential scanning calorimetry (DSC) experiments were performed using Q100 DSC from TA Instruments under nitrogen atmosphere. Wide-angle and small-angle X-ray scattering (WAXS and SAXS) experiments were performed by using a rotating anode generator (Rigaku Nanoviewer MicroMax) and a NanoStar-Bruker AXS setup working a sample-to-detector distance of 309 and 1046 mm, respectively. Both setups produced X-ray beam with a wavelength of 1.54 Å and were equipped with a homemade heating stages having a thermal stability of 0.1 °C for temperature dependence experiments.

Synthesis. *Synthesis of Ethynyl-Terminated P3HT (Ethynyl-P3HT).* Ethynyl-functionalized P3HT was synthesized according to the procedure described in the previous work. To a flame-dried 100 mL were added Schlenk flask 2,5-dibromo-3-hexyl thiophene (2 g, 6.13 mmol) and THF (8 mL). Isopropyl magnesium chloride (3.1 mL, 6.13 mmol) was added, and then the mixture solution was stirred at room temperature for 2 h under N_2 atmosphere. An additional 40 mL of THF and Ni(dppp)Cl_2 (0.184 g, 0.34 mmol) were added and stirred for 10 min. Then 3.7 mL (1.84 mmol, 30 mol % of monomer) of magnesium chloride (2.0 M in THF) was added, and the mixture was stirred for an additional 2 min. The mixture was poured into about 500 mL of methanol to precipitate the polymer. The collected polymer was dissolved in chloroform and precipitated in acetone again. The obtained polymer was dried under vacuum. ^{1}H NMR (400 MHz, $CDCl_3$): δ 0.91 (t, 3H), 1.34 (m, 6H), 1.69 (t, 2H), 2.80 (t, 2H), 3.53 (s, 1H), 6.97 (s, 1H).

Synthesis of Azido-Terminated PMMA (PMMA-N_3). Azido-terminated PMMA was prepared by ATRP initiated by 2-azidoethyl 2-bromoisobutyrate. Polymerization of methyl methacrylate was conducted in ethyl acetate solution at 90 °C using [Cu(I)Br]:[2-azidoethyl 2-bromoisobutyrate]:[2,2′-bipyridine] = 1:1:3 and [MMA]:[2-azidoethyl 2-bromoisobutyrate] = 50:1. First, 10 mL of ethyl acetate and 4.68 g (46.8 mmol) of methyl methacrylate (MMA) was added to a flame-dried 100 mL Schlenk flask. The solution was degassed by three freeze−pump−thaw cycles. Then, 44.0 g (2.82 mmol) of 2,2′-bipyridine was added with nitrogen purging, and the mixture was degassed by two freeze−pump−thaw cycles. Then, 0.13 g (0.94 mmol) of CuBr was added with nitrogen purging and degassed by twice freeze−pump−thaw cycles before addition of 0.22 g (0.94 mmol) of 2-azidoethyl 2-bromoisobutyrate at room temperature. After one more freeze−pump−thaw cycle, the mixture solution was stirred at 90 °C for 15 min. The resulting polymer solution was diluted with THF and passed through a basic alumina column to eliminate catalyst and then the polymer was isolated by precipitation into the mixture of methanol and water (1/1 = v/v). The polymer was characterized by NMR, FT-IR, and GPC after drying it under vacuum. ^{1}H NMR (400 MHz, $CDCl_3$): δ 0.83 (s, 3H), 1.81 (m, 2H), 3.46 (t, 2H), 3.59 (m, 3H), 3.76 (m, 3H), 4.11 (m, 2H).

Synthesis of P3HT-b-PMMA. Ethynyl-P3HT (0.36 g, 0.11 mmol, 1.2 equiv), PMMA-N_3 (0.2 g, 0.09 mmol, 1.0 equiv), and CuBr (0.12 mg, 0.9 mmol, 10 equiv) were added to a Schlenk flask. The flask was evacuated and backfilled three times with nitrogen before 40 mL of THF was added. After all reagents were dissolved in THF, PMDETA (0.15 g, 0.9 mmol, 10 equiv) was added to the flask. The mixture solution was stirred at 50 °C, and the completion of the reaction was monitored by GPC. The resulting solution was passed through a basic alumina column to remove catalyst and then the resulting polymer was precipitated in methanol. The obtained polymer was filtered through an extraction thimble and then washed by Soxhlet extraction with methanol, acetone, hexane, and chloroform. Acetone and hexane washing were used to get rid of homo-PMMA and P3HT, respectively. The last chloroform solution was concentrated and then poured into methanol to get the desired block copolymer. The polymer was dried in a vacuum oven.

Synthesis of P3HT-b^+-PMMA·I^-. A solution of P3HT-*b*-PMMA (160 mg, 2.8×10^{-2} mmol) and methyl iodide (16 mL, 240 mmol) in chloroform (8 mL) was stirred at for 3 days at 80 °C. The resulting polymer was precipitated in diethyl ether and dried in a vacuum oven.

Synthesis of P3HT-b^+-PMMA·NTf_2^-. A solution of P3HT-b^+-PMMA I^- (80 mg, 1.4×10^{-2} mmol) and $LiNTf_2$ (12 mg, 4.2×10^{-2} mmol) in THF (8 mL) was stirred for 3 days at room temperature. THF was removed and the solid was dissolved in chloroform. The polymer solution was washed with water and precipitated in diethyl ether. The obtained solid polymer was dried in a vacuum oven.

DOI: 10.1021/acs.macromol.6b02101
Macromolecules 2017, 50, 235−243

Table 1. Summary of the Characteristics of P3HT-*b*-PMMA

		DP_n[a]					DSC	
polymer	M_n[a] (g mol^{-1})	*m*	*n*	M_n[b] (g mol^{-1})	$Đ$[b]	f_{P3HT}[c] (%)	T_c (°C)[d] (1 °C/min)	T_c (°C)[d] (5 °C/min)
PMMA-N_3	2300	–	21	2600	1.44	–	–	–
ethynyl-P3HT	3400	20	–	3400	1.29	100		
P3HT-*b*-PMMA	5700	20	21	8900	1.71	61	170	155
P3HT-*b*$^+$-PMMA·I^-	–	20	21	–	–	–	160	137
P3HT-*b*$^+$-PMMA·NTf_2^-	–	20	21	–	–	–	–	112

[a]By NMR. [b]Calculated from GPC with PS standards. [c]The volume fraction of P3HT was calculated by using M_n calculated from ^{1}H NMR and the density of each polymer: ρ_{P3HT} = 1.11 g/mL and ρ_{PMMA} = 1.19 g/mL. [d]Below is mentioned the analysis cooling rate.

RESULTS AND DISCUSSION

ATRP of MMA was performed using 2-azidoethyl-2-bromoisobutyrate as an initiator, resulting in the formation of the azido-terminated PMMA-N_3. The degree of polymerization was obtained by comparing the integration value of methyl ester protons on PMMA repeat units at 3.59 ppm to that of methyl ester protons on the bromine-terminated end unit at 3.75 ppm (degree of polymerization = 21 and M_n = 2300 g·mol^{-1}) by proton nuclear magnetic resonance (^{1}H NMR, Figure S1). The molecular weight of PMMA-N_3 calculated by ^{1}H NMR was very close to that determined by steric exclusion chromatography (SEC) (M_n = 2600 g·mol^{-1}). These experimental results are in agreement with theoretical value estimated by ratio of monomer to catalyst and 51% conversion (M_n = 2550 g mol^{-1}). The presence of azido group was confirmed by the appearance of an azide stretching vibration peak at 2100 cm^{-1} in the FT-IR spectrum (Figure S2). Ethynyl-terminated P3HT was synthesized by GRIM polymerization as previously described except for its purification procedure.[27] Since the ethynyl-capped P3HT was unstable under ambient conditions, sequential Soxhlet extraction was eliminated. The obtained polymer was purified by precipitation twice from methanol and acetone. The degree of polymerization of ethynyl-P3HT was calculated to be 20 (M_n = 3400 g mol^{-1}) from the integration ratio of methylene protons b (2.80 ppm) to b′ + b″ (2.56 ppm) on thiophene units (Figure S3). ^{1}H NMR spectrum of the polymer also showed a singlet peak of ethynyl group, confirming the ethynyl group was successfully introduced to the end groups of P3HT. However, the integration value was higher than 1, indicating that the polymer could contain *α*,*ω*-end-capped product as previously mentioned by McCullough et al.[27]

Block copolymers were prepared by "click" coupling the ethynyl-P3HT with azido-terminated PMMA (Scheme S1). Since we could not exclude the possibility of difunctional end-capped P3HT, an excess of P3HT was used for a complete consumption of PMMA-N_3. Then, to control the duration of the coupling reaction, the cycloaddition was monitored via SEC until the peak associated with the elution of the block copolymer was no longer shifted. Two days were mandatory to reach final state. Acetone and hexane Soxhlet sequential extractions were used to get rid of homo PMMA and P3HT reagent, respectively. SEC analysis of the purified block copolymer exhibited a single peak indicating a single polymer with a dispersity of 1.7 and a distinctive shift in the retention time compared to starting polymers (Figure S4). A comparison by ^{1}H NMR of the integration value of the P3HT aromatic proton at 7.0 ppm (Figure S5) to that of PMMA methoxy protons at 3.59 ppm was in agreement with the homopolymers DP_n with a ratio of 1/1 (Table 1). A single peak corresponding to the proton on the triazole ring also appeared at 7.68 ppm, confirming the success of the coupling.

In addition, diffusion ordered NMR spectroscopy (DOSY) was performed to confirm that all ^{1}H signals belonged to the same macromolecule. As shown in Figure S6, ^{1}H signals corresponding to ethynyl-P3HT, azido-PMMA, and P3HT-*b*-PMMA had different diffusion coefficients and only one diffusion coefficient was observed from P3HT-*b*-PMMA, which allowed us to conclude that one single diblock copolymer was present in the sample and free of any homopolymers.

The triazole linker of the P3HT-*b*-PMMA was methylated with an excess of methyl iodide to yield the triazolium iodide (**P3HT-*b*$^+$-PMMA·I^-**). ^{1}H NMR spectra of the copolymers clearly confirmed the successful quaternization of the triazole groups. As shown in Figure 1, while the peak representing the proton of 1, 2, 3-triazole ring shifted from 7.68 to 9.18 ppm, a new peak corresponding to the methyl protons group appeared at 4.38 ppm. Finally, anion methathesis of **P3HT-*b*$^+$-PMMA·I^-** was performed with bis(trifluoromethane) sulfonimide lithium salt to obtain the copolymer having a (trifluoromethane) sulfonamide (**NTf_2^-**) as counteranions (**P3HT-*b*$^+$-PMMA·NTf_2^-**). The proton signals of the 1,2,3-triazolium ring and other groups adjacent to the 1,2,3-triazolium moiety (N^3−CH_3 and N^1−CH_2CH_2 groups) were shifted after anion exchange (Figure 1).

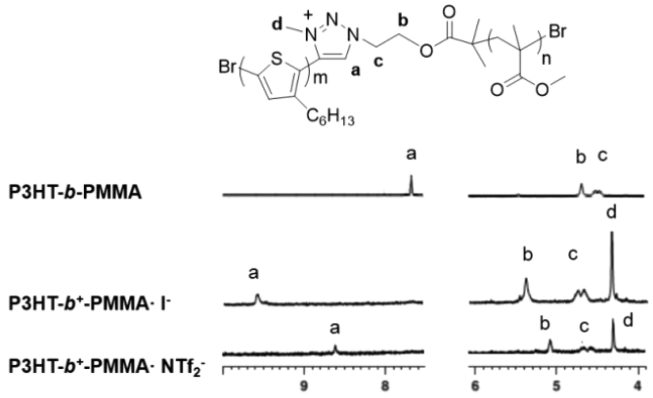

Figure 1. ^{1}H NMR spectra of 1,2,3-triazole- and 1,2,3-triazolium-linked BCPs.

The influence of the linker between blocks was recently explored by Bernard et al. where a PS-*b*-PMMA linked by supramolecular coupling with complementary associative oligoamide groups was synthesized (PS-*supra*-PMMA). The authors revealed differences in thin film morphologies between the covalent PS-*b*-PMMA and their PS-*supra*-PMMA.[28] In our study, the diblock self-assembly was investigated by atomic

DOI: 10.1021/acs.macromol.6b02101
Macromolecules 2017, 50, 235−243

force microscopy (AFM), small and wide-angle X-ray scattering (SAXS and WAXS), and differential scanning calorimetry (DSC).

The three copolymers SAXS patterns evolution with temperature showed that an annealing above 150 °C is necessary to find a peak around 0.35 nm^{-1} with an associated characteristic size of 18 nm pertaining to the diblock nanophase segregation (Figure 2 and temperature profiles in Figures S7–S9). It has to be noted that the order–disorder transition temperature was not reach at 210 °C. We could not heat further without risking the samples degradation starting at around 240 °C (the thermogravimetric analysis is presented in Figure S10).

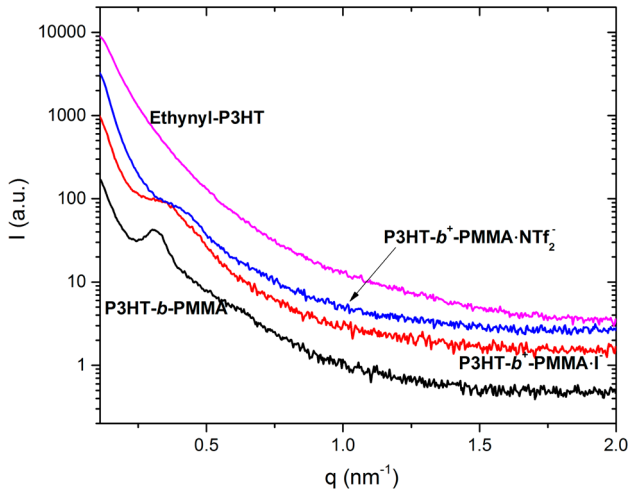

Figure 2. SAXS spectra of the P3HT homopolymer and the three diblock copolymers acquired at room temperature after a thermal annealing at 200 °C.

Thin films of the three BCPs (around 300 nm thick) were prepared by spin-coating from toluene solution (10 mg/mL, 1.1 w%) onto Si wafers, and thermally annealed at 80 °C for 1 h and then 200 °C for 10 min. The surface morphology of the thin films was observed by AFM (Figure 3 and Figures S11–12). The annealing temperature was set above the melting point of P3HT but below the order–disorder transition temperature allowing PH3T segment to move to some extent. As seen in Figure 3a, P3HT exhibited randomly oriented fibrillar structure that is typical of P3HT morphology due to its crystallization. On the other hand, the neutral BCP (P3HT-*b*-PMMA) showed densely packed nanofibrils (Figure 3b) as expected from the literature.[29−32]

The AFM images collected on **P3HT-*b*$^+$-PMMA·I$^-$** showed elongated and nicely ordered well-defined fibrils (Figure 3 c). The dimension of the well-defined and ordered fibrils period is 15 nm in agreement with the SAXS analysis. A theoretical all-trans chain length of the P3HT block can be obtained by multiplying the monomer unit length (0.38 nm) with the degree of polymerization of P3HT (N_{P3HT} = 20) to give a rod length of 7.6 nm. This result demonstrates that the molecular organization of **P3HT-b$^+$-PMMA·I$^-$** chains in the fibrils consist of a monolayer of the diblock.

Finally, the **P3HT-*b*$^+$-PMMA·NTf$_2^-$** AFM images were greatly different from other two BCPs (Figure 3 d). Although a clear nanophase segregation could be seen with curved domains, the exact morphology could not be identified. The SAXS data do not provide here further information to identify the morphology.

The morphology of P3HT homopolymer has been known to be affected by their strong $\pi-\pi$ interaction between the conjugated backbones, leading to the formation of highly ordered molecular organizations. Therefore, in addition to the enthalpic interaction characterized by the Flory–Huggins interaction parameter χ, the molecular arrangement of P3HT-based block copolymers in the condensed phase is also affected by the Maier–Saupe parameter (μ) representing the strength of the orientational interaction favoring the alignment of the rods (π-stacking).[33] The AFM images of the charged copolymer demonstrated that the self-assembly of BPCs can be tuned by introducing a charged linker between the two blocks. The electrostatic interactions between ionic linkers is another driving force in the system that disturb the original organization.

To investigate further the influence of the charge on the copolymer self-assembly, WAXS analysis were performed. As shown in Figure 4, the WAXS patterns of both the P3HT homopolymer and the neutral P3HT-*b*-PMMA exhibited similar diffraction peaks, which correspond to the reflections from the crystallographic planes (100) at 3.75 nm^{-1}, (200) at 7.5 nm^{-1}, (300) at 11.25 nm^{-1}, and (020)/(002) at 16.5 nm^{-1} associated with a regular form I crystal of an orthorhombic unit cell.[34] As shown by Tashiro et al., the peak at 16.5 nm^{-1} is a superposition of the (020) and a weak (002) reflection.[31] For these polymers, the corresponding *d*-spacings of (100) and (020)/(002) planes were 16.7 and 3.8 Å, respectively. The (100) reflection corresponds to the interchains distance separated by the hexyl side chain of P3HT, the (020) reflection corresponds to the distance of the π-stacking between the main chain monomer units and finally the (002) reflections is related to the distance between hexyl chains along the backbone (i.e., the monomer size along the chain). The **P3HT-*b*$^+$-PMMA·I$^-$** WAXS signals showed the same peaks plus the (400) plane at 15.2 nm^{-1} and (120) plane at 17.2 nm^{-1} indicating a higher ordering in the P3HT crystals compared with the homopolymer and P3HT-*b*-PMMA.[35] The dipole presents at the block junction could induce this longer range organization. Moreover another signal appeared at 9.35 nm^{-1} when the sample was annealed above 200 °C (see Figure S13) which is not fully understood but could be linked to the 1, 2, 3-triazolium iodide degradation as discussed below.

Surprisingly **P3HT-*b*$^+$-PMMA·NTf$_2^-$** adopted a very different behavior. The crystallinity observed when increasing temperature from 50 to 150 °C vanished at 200 °C above the melting temperature of the P3HT block (Figure S14). When the sample was cooled down, the WAXS spectrum only exhibits a broad diffuse peak at about 4 nm^{-1}, indicating a poor packing of P3HT segments and no recrystallization (Figure 4).

Herein, we have to mention that the thermal stability of the ester linkage in vicinity of 1,2,3-triazole ring was confirmed by GPC after thermal annealing of BCPs. Indeed, some homopolymers might be formed due to the ester linkage thermal degradation and in this case, the system could no longer pure BCP, but a blend of block copolymer and homopolymers (Figure S15).

To confirm this surprising lost of crystallinity, differential scanning calorimetry was performed on the samples. After an initial isotherm at 200 °C during 10 min the temperature was cooled to 40 °C at 1 °C/min to mimic the condition of the WAXS experiment (Figure 5 a). The neutral P3HT-*b*-PMMA

DOI: 10.1021/acs.macromol.6b02101
Macromolecules 2017, 50, 235–243

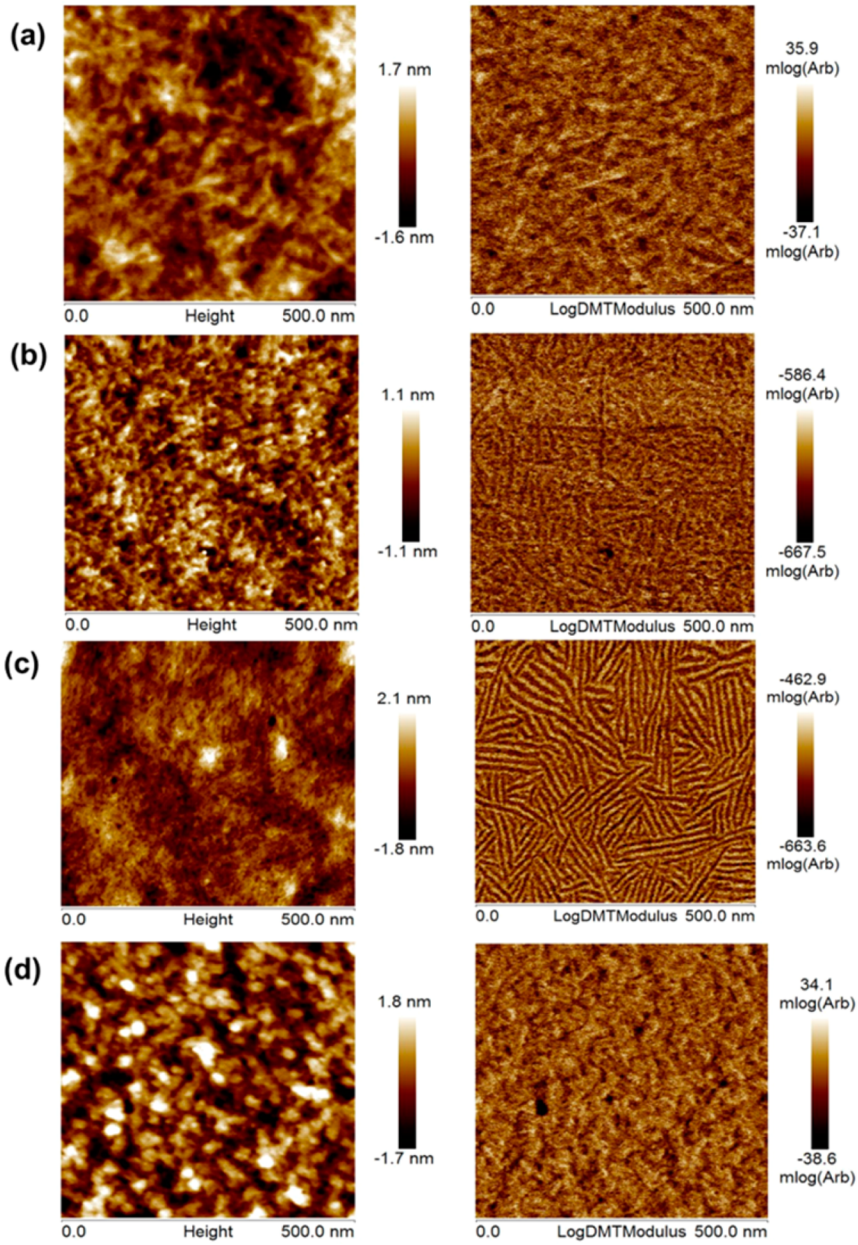

Figure 3. PeakForce QNM-mode AFM images of ethynyl-P3HT (a), P3HT-*b*-PMMA (b), P3HT-b^+-PMMA·I^- (c), and P3HT-b^+-PMMA·NTf_2^- (d) films thermally annealed at 200 °C.

analysis showed an exothermic peak pertaining to a recrystallization at 170 °C. For the charged copolymer the recrystallization of **P3HT-b^+-PMMA·I^-** was switched to 160 °C and no significant recrystallization was observed for **P3HT-b^+-PMMA·NTf_2^-** as suggested by the WAXS pattern and meaning that the P3HT phase was amorphous.

The samples were then analyzed after an isotherm at 200 °C during 10 min and a cooling to 40 °C at 5 °C/min (Figure 5 b). The neutral copolymer and **P3HT-b^+-PMMA·I^-** thermograms were quite similar to the previous ones except for a slight shift of the crystallization temperature toward the low values due to the experimental conditions (Table 1). For **P3HT-b^+-PMMA·NTf_2^-** was observed this time an exothermic peak at 110 °C just around the PMMA glass transition temperature.

On the heating scan (ramp 10 °C/min, Figure S16, performed after a cooling treatment at 1 °C/min)), the three copolymers exhibited a glass transition temperature at 105 °C pertaining to the PMMA phase. A single endothermic peak around 170 °C corresponding to the melting of P3HT crystals was also detected on the neutral P3HT-*b*-PMMA and **P3HT-b^+-PMMA·I^-** thermograms. Surprisingly, a weak endothermic peak was observed for the **P3HT-b^+-PMMA·NTf_2^-**. If no crystallization was observed during the cooling, no melting should be detected. Modulated DSC (MDSC) was then performed on the **P3HT-b^+-PMMA·NTf_2^-** to finely identify the phenomena involved in its thermic behavior.

Modulated DSC measures both heat flow and heat capacity in a single experiment by superimposing a modulated heating rate on top of a linear one. As a consequence it is possible to identify kinetic processes such as crystallization. Figure 6a shows the MDSC signals of the cooling of **P3HT-b^+-PMMA·NTf_2^-** from 200 to 40 °C at 5 °C/min. It can be seen that P3HT crystallization was identified at 110 °C on the nonreversible signal whereas PMMA Tg was detected at the

DOI: 10.1021/acs.macromol.6b02101
Macromolecules 2017, 50, 235−243

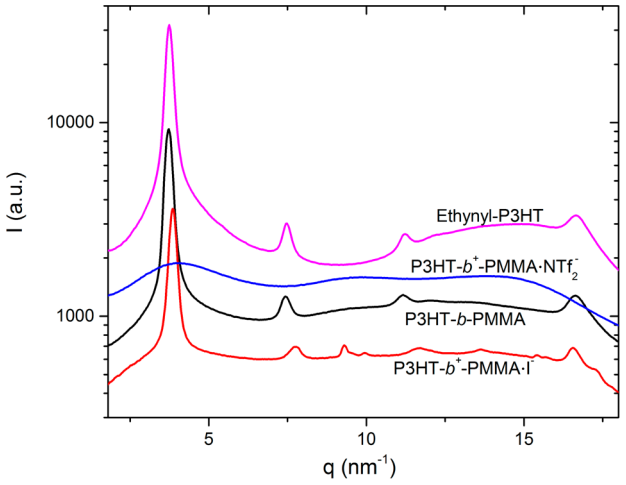

Figure 4. WAXS spectra of the P3HT homopolymer and the three diblocks acquired at room temperature after a thermal annealing at 200 °C.

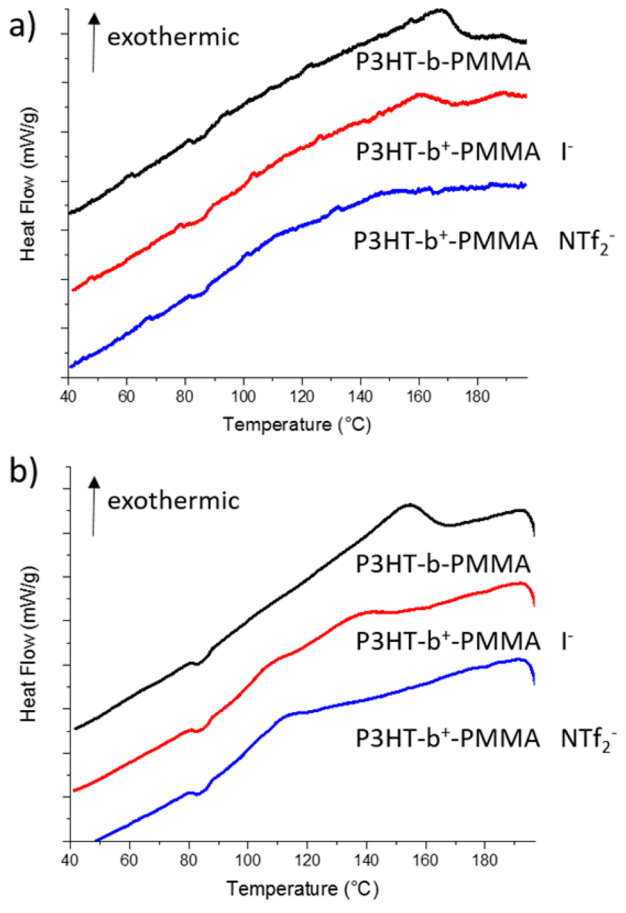

Figure 5. DSC thermogram of the copolymers on the cooling scan from 200 to 40 °C at (a) 1 °C/min and (b) 5 °C/min.

same temperature on the reversible signal. As a consequence P3HT crystal formation could be impeded by the lack of mobility brought by the PMMA in its glassy state.

Figure 6b presents the MDSC signals of the heating scan of **P3HT-*b*$^+$-PMMA·NTf$_2^-$** from 40 to 200 °C at 10 °C/min after an initial cooling treatment from 200 to 40 °C at 1 °C/min, i.e., where no crystallization was observed. Importantly, the nonreversible signal shows an exothermic cold crystallization

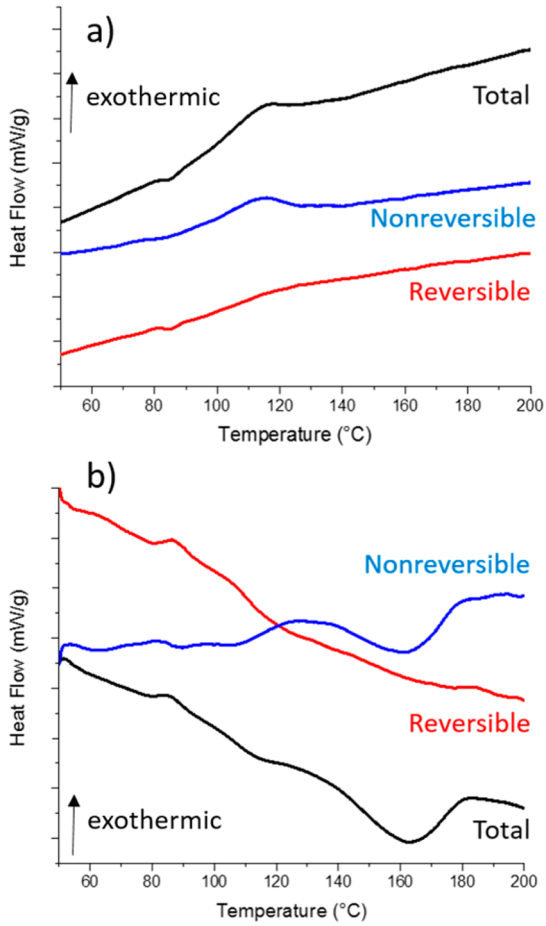

Figure 6. DSC traces of **P3HT-*b*$^+$-PMMA·NTf$_2^-$**: (a) Cooling cycle from 200 to 40 °C at 5 °C/min; (b) heating cycle from 40 to 200 °C at 10 °C/min after an initial cooling treatment from 200 to 40 °C at 1 °C/min, where no recrystallization was observed.

starting at 110 °C prior to the melting endothermic peak at 165 °C. This suggest that in this system the P3HT crystal formation, which is initially inhibited by the glassy state of PMMA chains during a cooling at 1 °C/min, is carried out during the annealing once PMMA segments are in the rubber state.

On the basis of the results of X-ray scattering, AFM and (M)DSC, the organization of the copolymer is now discussed. Because of the incompatibility between P3HT and PMMA, the χ value is expected to be high enough to ensure nanophase segregation.[36] Lin et al. suggested the Flory−Huggins parameter between P3HT and PMMA as $\chi = 56.370/T + 0.0433$.[14] With this equation, the χ value of our BCP is 0.24 at 293 K, and χN equals 13, where $N = 54$ (one PMMA monomer is used as reference volume). Lin et al. also calculated the value of the μ parameter for P3HT, $\mu = -0.3 + 180/T$. At 293 K the G parameter (μ/χ) equal 1.3 resulting in stronger rod−rod interactions than microphase separation and fibril like morphology are finally observed (with $f_{P3HT} = 0.61$). When the neutral P3HT-*b*-PMMA sample is annealed, the G parameter will decrease below 1 but during the cooling process, as the copolymer will undergo crystallization before PMMA vitrification, the rod−rod interaction will drive the morphology.

The WAXS and DSC results have demonstrated that the introduction of an ion pair at the junction of the two block

DOI: 10.1021/acs.macromol.6b02101
Macromolecules 2017, 50, 235−243

disturb the crystallization. Yoo et al. have already reported such a behavior in poly(butylene adipate) ionomers where they showed a substantial decrease in the fusion enthalpy when the number of ion per chains was increased.[37] In our system, the effect is minor when I^- is used as the counterion and result in a long-range fibrils organization. Montarnal et al. have studied the influence of an ion pair at the center of a PDMS-*b*-PEO and observed that the order−disorder temperature was increased compared to the neutral copolymer.[24] They attributed this behavior to an increase in the χ factor. In our case the ion pairs decreased the influence of μ and the diblock phase segregation becomes predominant. Moreover, as previously observed,[24] we noted that 1, 2, 3-triazolium iodide within the BCP underwent demethylation at 200 °C (Figure S17). Therefore, the experimental results suggest that methyl group on the 1, 2, 3-triazolium unit with iodide could serve as a promoter of the diblock phase segregation to allow highly ordered well-defined structures, and can subsequently be removed during thermal annealing.[38,39]

The effect on the self-assembly of the copolymer by introducing an ion pair with NTf_2^- as the counterion, is major. Indeed, a significant inhibition of the crystallization is observed compared with the neutral and iodide BCPs associated with a decrease of the influence of μ. At a cooling rate of 1 °C/min the crystallization was not observed and at 5 °C/min the crystallization temperature appeared but so close to the glass transition temperature of PMMA that the P3HT organization is impeded by the glassy chains of PMMA. The steric effect due to the large NTf_2^- counterion could be considered to explain the morphology deviation. The mobility of P3HT chains in the vicinity of multiplets formed by large ions could be restricted to prevent $\pi-\pi$ stacking. The effect was even more pronounced since this NTf_2^- counteranion hydrophobicity (due to its fluorine atoms) and its weak cation coordination (compared to iodide[40]) could then favor a swelling of the hydrophobic P3HT phase (and not the more hydrophilic PMMA) and inhibit crystallization. As a consequence in **P3HT-*b*$^+$-PMMA·NTf$_2^-$**, the Maier−Saupe μ and the *G* parameters drastically decreased compared to the neutral polymer and their influence on the film morphology vanished.

The influence of the cooling rate on the crystallization is counterintuitive since a crystal formation usually benefits from a slow cooling.[41] Here we observe a competition between the glass transition and the crystallization on which the cooling rate as an effect. This untypical cooling rate behavior is currently running in our laboratory on different rod−coil BCPs.

CONCLUSION

In conclusion, we have described a synthetic strategy to manipulate the self-assembly behavior of BCPs to reach various nanostructures. More precisely, the $\pi-\pi$ interaction, found in the conjugated block P3HT and leading to disordered fibril morphology, can be overcome by introducing an additional ionic interaction located in between the two blocks of the rod−coil BCPs. Huisgen cycloaddition of two functional homopolymers leaded to well-defined BCPs with an ionizable group on the linking unit. AFM, SAXS, and WAXS have shown that the presence of ionic groups brought an additional driving force in the system and induced changes in the self-assembly from the neutral BCP. The 1,2,3-triazolium-based BCP with iodide as the counterion exhibited highly organized well-defined fibrils, as the diblock phase segregation becomes predominant over the rod−rod interaction. Moreover, thermally unstable 1,2,3-triazolium iodide underwent demethylation, leading back to the neutral copolymer materials.

When the more stable and larger NTf_2^- was used as counterion, the P3HT phase was disrupted and no crystallization was observed. As a consequence, the fibril morphology was replaced by a nonidentified and curved morphology dictated by the diblock segregation and the ion pairs aggregation.

This methodology could be a useful strategy to open the range of nanomorphologies reachable with a semiconducting polymer for electronic or photovoltaic applications.

ASSOCIATED CONTENT

Supporting Information

The Supporting Information is available free of charge on the ACS Publications website at DOI: 10.1021/acs.macromol.6b02101.

Experimental details and additional characterization data (PDF)

AUTHOR INFORMATION

Corresponding Author

*(L.B.) E-mail: laurent.billon@univ-pau.fr. Fax: 00 33 5 59 40 76 22. Telephone: 00 33 5 59 40 76 09.

ORCID

Laurent Billon: 0000-0003-0999-899X

Funding

E.J.'s position was financially supported by a CDAPP fellowship. SEC, NMR, and AFM analyses were supported by a public grant overseen by the French National Research Agency ANR-10-EQPX-16 XYLOFOREST.

Notes

The authors declare no competing financial interest.

ACKNOWLEDGMENTS

Dr. Abdel Khoukh is acknowledged for fruitful discussion on NMR analysis.

REFERENCES

(1) Tseng, Y. C.; Darling, S. B. Block Copolymer Nanostructures for Technology. *Polymers* **2010**, *2* (4), 470−489.

(2) Li, L.; Shen, X.; Hong, S. W.; Hayward, R. C.; Russell, T. P. Fabrication of Co-continuous nanostructured and porous polymer membranes: Spinodal decomposition of homopolymer and random copolymer blends. *Angew. Chem., Int. Ed.* **2012**, *51* (17), 4089−4094.

(3) Majewski, P. W.; Gopinadhan, M.; Jang, W. S.; Lutkenhaus, J. L.; Osuji, C. O. Anisotropic ionic conductivity in block copolymer membranes by magnetic field alignment. *J. Am. Chem. Soc.* **2010**, *132* (49), 17516−17522.

(4) De Cuendias, A.; Hiorns, R. C.; Cloutet, E.; Vignau, L.; Cramail, H. Conjugated rod-coil block copolymers and optoelectronic applications. *Polym. Int.* **2010**, *59* (11), 1452−1476.

(5) Holyst, R.; Schick, M. Correlations in a rigid-flexible diblock copolymer system. *J. Chem. Phys.* **1992**, *96* (1), 730−739.

(6) Müller, M.; Schick, M. Ordered Phases in Rod−Coil Diblock Copolymers. *Macromolecules* **1996**, *29* (27), 8900−8903.

(7) Olsen, B. D.; Segalman, R. A. Nonlamellar phases in asymmetric rod-coil block copolymers at increased segregation strengths. *Macromolecules* **2007**, *40* (19), 6922−6929.

(8) Qian, L.; Yang, J.; Zhou, R.; Tang, A.; Zheng, Y.; Tseng, T. K.; Bera, D.; Xue, J.; Holloway, P. H. Hybrid polymer-CdSe solar cells with a ZnO nanoparticle buffer layer for improved efficiency and lifetime. *J. Mater. Chem.* **2011**, *21* (11), 3814−3817.

DOI: 10.1021/acs.macromol.6b02101
Macromolecules 2017, 50, 235−243

(9) Lin, S.-H.; Ho, C.-C.; Su, W.-F. Cylinder-to-gyroid phase transition in a rod-coil diblock copolymer. *Soft Matter* **2012**, *8* (18), 4890−4893.
(10) Alemseghed, M. G.; Servello, J.; Hundt, N.; Sista, P.; Biewer, M. C.; Stefan, M. C. Amphiphilic block copolymers containing regioregular poly(3-hexylthiophene) and poly(2-ethyl-2-oxazoline). *Macromol. Chem. Phys.* **2010**, *211* (12), 1291−1297.
(11) Erothu, H.; Kolomanska, J.; Johnston, P.; Schumann, S.; Deribew, D.; Toolan, D. T. W.; Gregori, A.; Dagron-Lartigau, C.; Portale, G.; Bras, W.; Arnold, T.; Distler, A.; Hiorns, R. C.; Mokarian-Tabari, P.; Collins, T. W.; Howse, J. R.; Topham, P. D. Synthesis, thermal processing, and thin film morphology of poly(3-hexylthiophene)-poly(styrenesulfonate) block copolymers. *Macromolecules* **2015**, *48* (7), 2107−2117.
(12) Javier, A. E.; Patel, S. N.; Hallinan, D. T., Jr; Srinivasan, V.; Balsara, N. P. Simultaneous electronic and ionic conduction in a block copolymer: Application in lithium battery electrodes. *Angew. Chem., Int. Ed.* **2011**, *50* (42), 9848−9851.
(13) Lee, Y. H.; Yen, W. C.; Su, W. F.; Dai, C. A. Self-assembly and phase transformations of π-conjugated block copolymers that bend and twist: From rigid-rod nanowires to highly curvaceous gyroids. *Soft Matter* **2011**, *7* (21), 10429−10442.
(14) Lin, S.-H.; Wu, S.-J.; Ho, C.-C.; Su, W.-F. Rational Design of Versatile Self-Assembly Morphology of Rod−Coil Block Copolymer. *Macromolecules* **2013**, *46* (7), 2725−2732.
(15) Higashihara, T.; Ueda, M. Synthesis and characterization of a novel coil-rod-coil triblock copolymers comprised of regioregular poly(3-hexylthiophene) and poly(methyl methacrylate) segments. *React. Funct. Polym.* **2009**, *69* (7), 457−462.
(16) Moon, H. C.; Anthonysamy, A.; Kim, J. K.; Hirao, A. Facile synthetic route for well-defined poly(3-hexylthiophene)-block- poly(methyl methacrylate) copolymer by anionic coupling reaction. *Macromolecules* **2011**, *44* (7), 1894−1899.
(17) Ho, V.; Boudouris, B. W.; Segalman, R. A. Tuning Polythiophene Crystallization through Systematic Side Chain Functionalization. *Macromolecules* **2010**, *43* (19), 7895−7899.
(18) Sirringhaus, H.; Tessler, N.; Friend, R. H. Integrated optoelectronic devices based on conjugated polymers. *Science* **1998**, *280* (5370), 1741−1744.
(19) Irwin, M. T.; Hickey, R. J.; Xie, S.; Bates, F. S.; Lodge, T. P. Lithium Salt-Induced Microstructure and Ordering in Diblock Copolymer/Homopolymer Blends. *Macromolecules* **2016**, *49* (13), 4839−4849.
(20) Bazuin, C. G.; Eisenberg, A. Modification of polymer properties through ion incorporation. *Ind. Eng. Chem. Prod. Res. Dev.* **1981**, *20* (2), 271−286.
(21) Capek, I. Nature and properties of ionomer assemblies. II. *Adv. Colloid Interface Sci.* **2005**, *118* (1−3), 73−112.
(22) Schadler, V.; Wiesner, U. Salt-controlled lamellar spacing in ionically end-capped symmetric diblock copolymers. *Macromolecules* **1997**, *30* (21), 6698−6701.
(23) Schöps, M.; Leist, H.; DuChesne, A.; Wiesner, U. Salt-Induced Switching of Microdomain Morphology of Ionically Functionalized Diblock Copolymers. *Macromolecules* **1999**, *32* (8), 2806−2809.
(24) Luo, Y.; Montarnal, D.; Treat, N. J.; Hustad, P. D.; Christianson, M. D.; Kramer, E. J.; Fredrickson, G. H.; Hawker, C. J. Enhanced Block Copolymer Phase Separation Using Click Chemistry and Ionic Junctions. *ACS Macro Lett.* **2015**, *4* (12), 1332−1336.
(25) Handa, N. V.; Serrano, A. V.; Robb, M. J.; Hawker, C. J. Exploring the synthesis and impact of end-functional poly(3-hexylthiophene). *J. Polym. Sci., Part A: Polym. Chem.* **2015**, *53* (7), 831−841.
(26) Mudraboyina, B. P.; Obadia, M. M.; Allaoua, I.; Sood, R.; Serghei, A.; Drockenmuller, E. 1,2,3-Triazolium-Based Poly(ionic liquid)s with Enhanced Ion Conducting Properties Obtained through a Click Chemistry Polyaddition Strategy. *Chem. Mater.* **2014**, *26* (4), 1720−1726.
(27) Jeffries-El, M.; Sauvé, G.; McCullough, R. D. Facile synthesis of end-functionalized regioregular poly(3-alkylthiophene)s via modified Grignard metathesis reaction. *Macromolecules* **2005**, *38* (25), 10346−10352.
(28) Montarnal, D.; Delbosc, N.; Chamignon, C.; Virolleaud, M. A.; Luo, Y.; Hawker, C. J.; Drockenmuller, E.; Bernard, J. Highly Ordered Nanoporous Films from Supramolecular Diblock Copolymers with Hydrogen-Bonding Junctions. *Angew. Chem., Int. Ed.* **2015**, *54* (38), 11117−11121.
(29) Pascui, O. F.; Lohwasser, R.; Sommer, M.; Thelakkat, M.; Thurn-Albrecht, T.; Saalwachter, K. High Crystallinity and Nature of Crystal-Crystal Phase Transformations in Regioregular Poly(3-hexylthiophene). *Macromolecules* **2010**, *43* (22), 9401−9410.
(30) Shetter, J. A. Effect of stereoregularity on the glass temperatures of a series of polyacrylates and polymethacrylates. *J. Polym. Sci., Part B: Polym. Lett.* **1963**, *1* (5), 209−213.
(31) Tashiro, K.; Ono, K.; Minagawa, Y.; Kobayashi, M.; Kawai, T.; Yoshino, K. Structure and thermochromic solid-state phase transition of poly(3-alkylthiophene). *J. Polym. Sci., Part B: Polym. Phys.* **1991**, *29* (10), 1223−1233.
(32) Lim, H.; Chao, C. Y.; Su, W. F. Modulating Crystallinity of Poly(3-hexylthiophene) via Microphase Separation of Poly(3-hexylthiophene)-Polyisoprene Block Copolymers. *Macromolecules* **2015**, *48* (10), 3269−3281.
(33) Pryamitsyn, V.; Ganesan, V. Self-assembly of rod-coil block copolymers. *J. Chem. Phys.* **2004**, *120* (12), 5824−5838.
(34) Prosa, T. J.; Winokur, M. J.; Moulton, J.; Smith, P.; Heeger, A. J. X-ray structural studies of poly(3-alkylthiophenes): an example of an inverse comb. *Macromolecules* **1992**, *25* (17), 4364−4372.
(35) Wu, Z.; Petzold, A.; Henze, T.; Thurn-Albrecht, T.; Lohwasser, R. H.; Sommer, M.; Thelakkat, M. Temperature and Molecular Weight Dependent Hierarchical Equilibrium Structures in Semiconducting Poly(3-hexylthiophene). *Macromolecules* **2010**, *43* (10), 4646−4653.
(36) Lim, H.; Huang, K.-T.; Su, W.-F.; Chao, C.-Y. Facile Syntheses, Morphologies, and Optical Absorptions of P3HT Coil-Rod-Coil Triblock Copolymers. *J. Polym. Sci., Part A: Polym. Chem.* **2010**, *48* (15), 3311−3322.
(37) Yoo, Y. T.; Lee, B. J.; Han, S. I.; Im, S. S.; Kim, D. K. Physical properties and biodegradation of poly(butylene adipate) ionomers. *Polym. Degrad. Stab.* **2003**, *79* (2), 257−264.
(38) Ho, C. C.; Wu, S. J.; Lin, S. H.; Darling, S. B.; Su, W. F. Kinetically Enhanced Approach for Rapid and Tunable Self-Assembly of Rod-Coil Block Copolymers. *Macromol. Rapid Commun.* **2015**, *36* (14), 1329−1335.
(39) RamachandraRao, V. S.; Gupta, R. R.; Russell, T. P.; Watkins, J. J. Enhancement of diblock copolymer ordering kinetics by supercritical carbon dioxide annealing. *Macromolecules* **2001**, *34* (23), 7923−7925.
(40) Zhang, Q.; Liu, S.; Li, Z.; Li, J.; Chen, Z.; Wang, R.; Lu, L.; Deng, Y. Novel cyclic sulfonium-based ionic liquids: Synthesis, characterization, and physicochemical properties. *Chem. - Eur. J.* **2009**, *15* (3), 765−778.
(41) Schawe, J. E. K. Cooling rate dependence of the crystallinity at nonisothermal crystallization of polymers: A phenomenological model. *J. Appl. Polym. Sci.* **2016**, *133* (6), 42977.

DOI: 10.1021/acs.macromol.6b02101
Macromolecules 2017, 50, 235−243

Supporting Information

Self-assembly of Ionizable "clicked" P3HT-*b*-PMMA Copolymers: ionic bonding group/counter ion effects on the morphology

Eunkyung Ji,[†] Virginie Pellerin,[†] Laurent Rubatat[†], Eric Grelet,[‡] Antoine Bousquet,[†] Laurent Billon*[†].

[†]IPREM CNRS-UMR 5254, Equipe de Physique et Chimie des Polymères, Université de Pau et des Pays de l'Adour, Hélioparc, 2 avenue Président Angot, 64053 Pau Cedex 9, France and [‡]Université de Bordeaux, CNRS, Centre de Recherche Paul-Pascal, 115 Avenue Schweitzer, 33600 Pessac, France

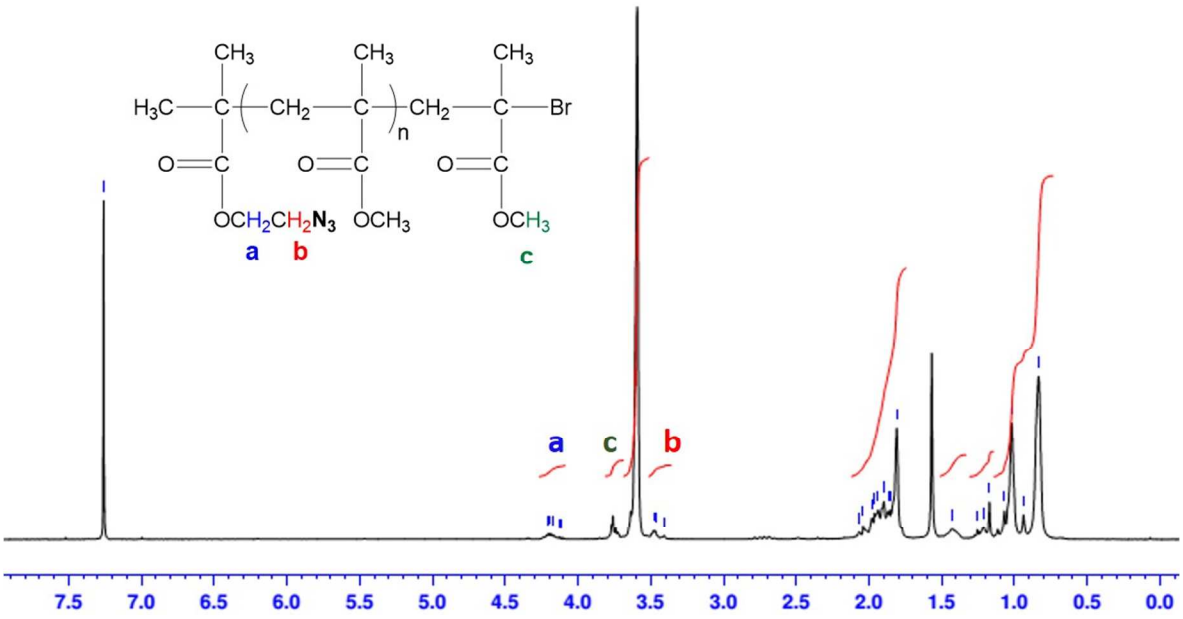

Figure S1. NMR spectra of PMMA-N_3.

ATRP of MMA was performed using 2-azidoethyl 2-bromoisobutyrate as an initiator, resulting in the formation of the azido-terminated PMMA-N_3. The degree of polymerization was obtained by comparing the integration value of methyl ester protons on PMMA repeat units at 3.59 ppm to that of methyl ester protons on the bromine-terminated end unit at 3.75 ppm. ^{1}H NMR (400 MHz, $CDCl_3$): δ 0.83 (s, 3H), 1.81 (m, 2H), 3.46 (t, 2H), 3.59 (m, 3H), 3.76 (m, 3H), 4.11 (m, 2H).

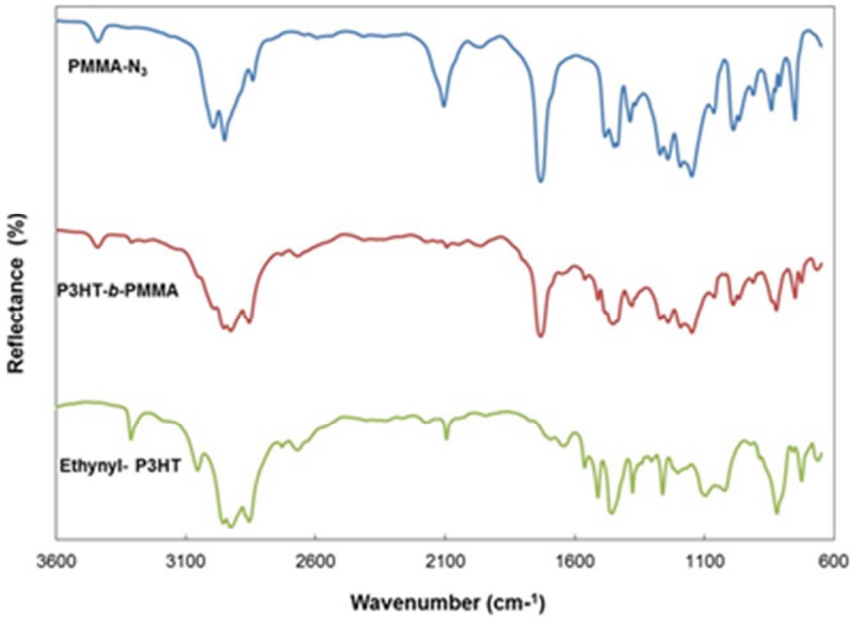

Figure S2. FTIR spectra of ethynyl P3HT, PMMA-N_3, and P3HT-*b*-PMMA.

The presence of azido group was confirmed by the appearance of an azide stretching vibration peak at 2 100 cm^{-1} in the FT-IR spectrum (Figure S2). This peak disappear after coupling with ethynyl P3HT.

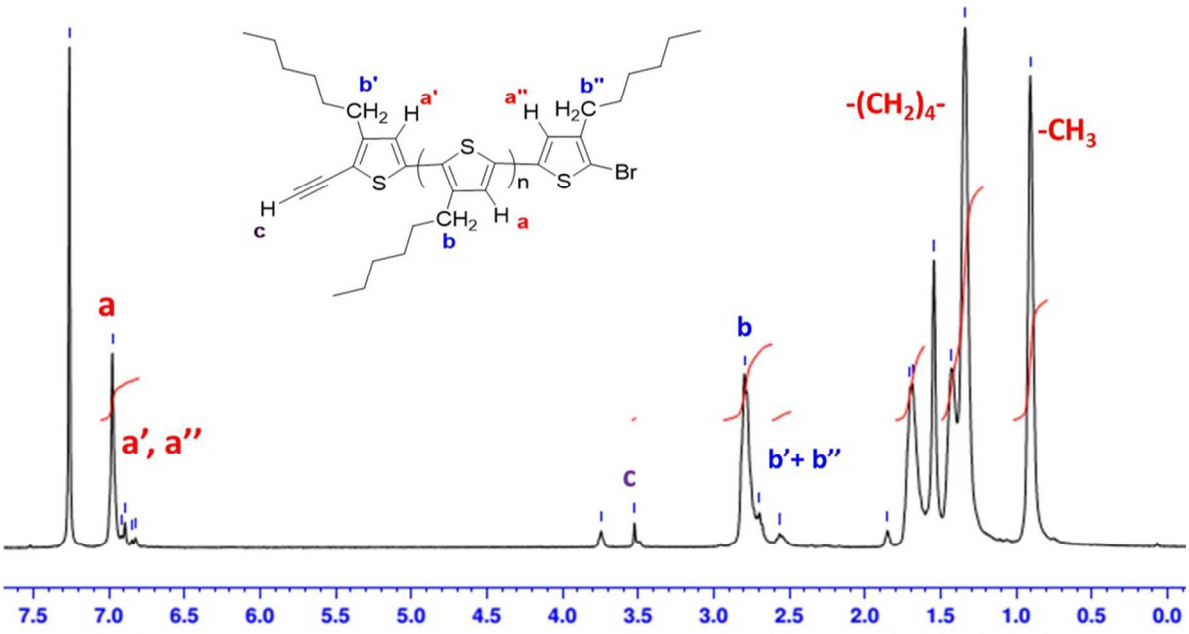

Figure S3. NMR spectrum of ethynyl P3HT.

The degree of polymerization of ethynyl-P3HT was calculated to be 20 from the integration ratio of methylene protons b (2.80 ppm) to b′+b″ (2.56 ppm) on thiophene units. ^{1}H NMR spectrum of the polymer also showed a singlet peak of ethynyl group, confirming the ethynyl group was successfully introduced to the end groups of P3HT. ^{1}H NMR (400 MHz, $CDCl_3$): δ 0.91 (t, 3H), 1.34 (m, 6H), 1.69 (t, 2H), 2.80 (t, 2H), 3.53 (s, 1H), 6.97 (s, 1H).

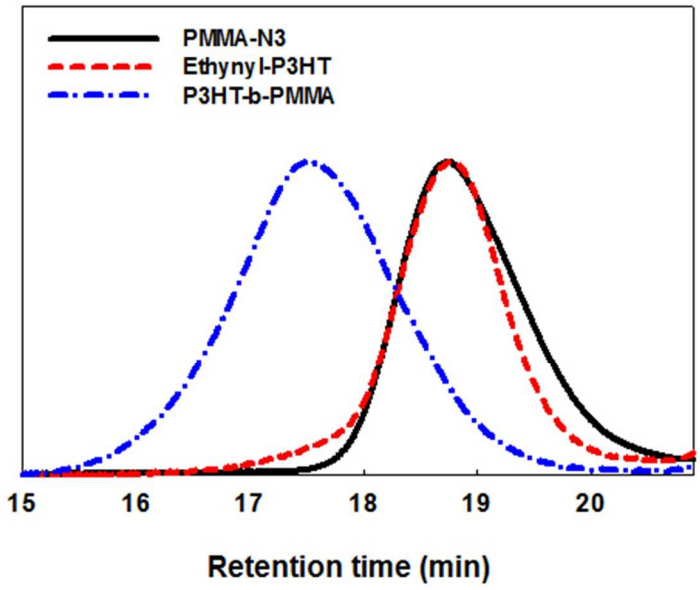

Figure S4. GPC traces of end-functionalized PMMA-N_3, ethynyl-P3HT, and their block copolymer P3HT-*b*-PMMA after click chemistry.

The completion of click coupling was monitored by SEC until the peak associated with the elution of the block copolymer was no longer shifted.

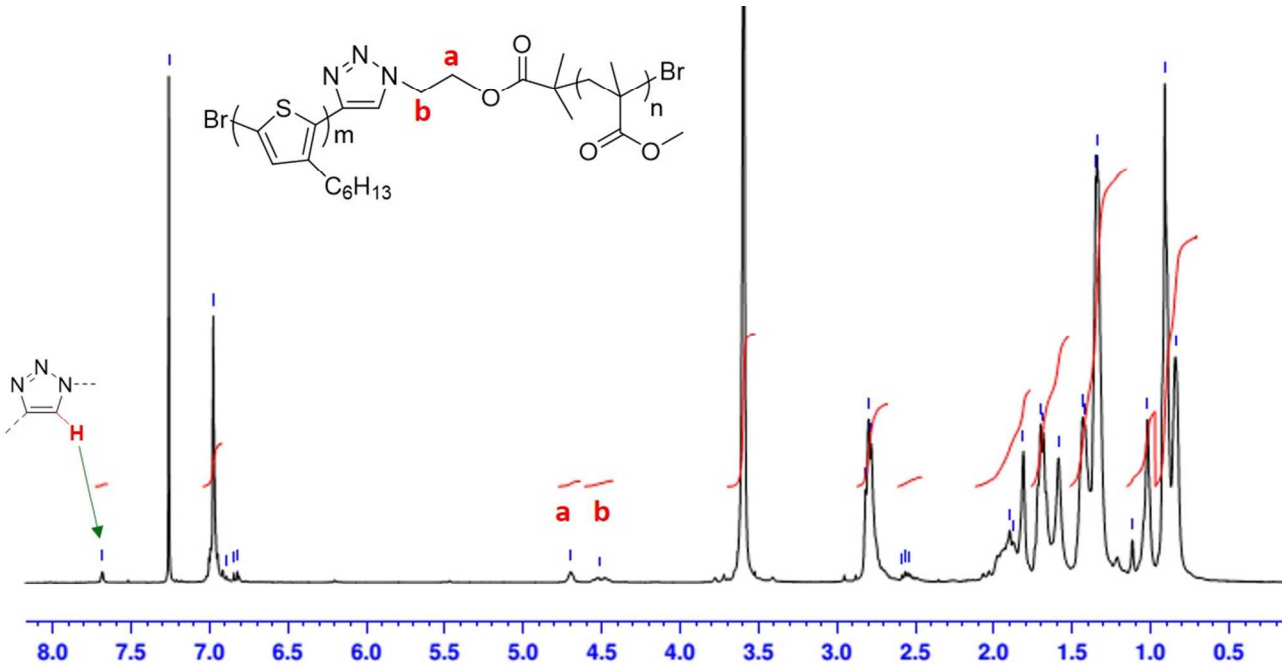

Figure S5. ^{1}H NMR spectrum of P3HT-*b*-PMMA.

A comparison by ^{1}H NMR of the integration value of the P3HT aromatic proton at 7.0 ppm (Figure S5) to that of PMMA methoxy protons at 3.59 ppm was in agreement with the homopolymers DP_n with a ratio of 1/1. A single peak corresponding to the proton on the triazole ring also appeared at 7.68 ppm, confirming the success of the coupling.

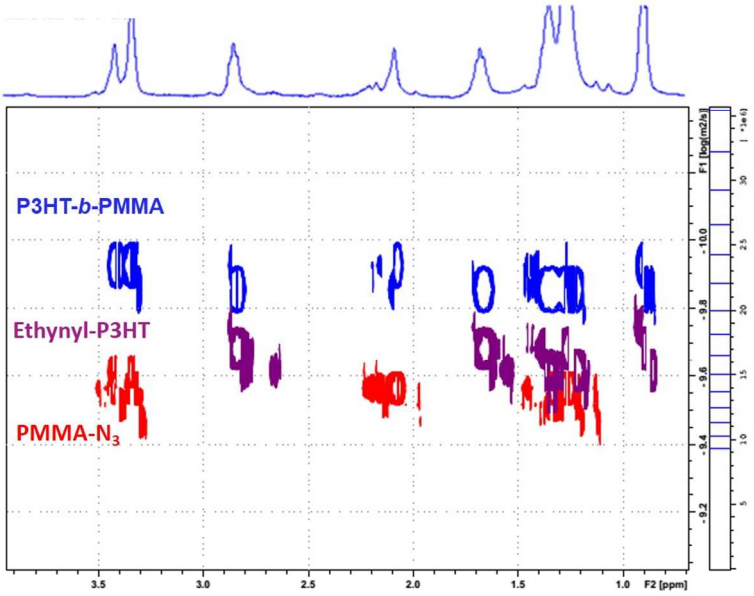

Figure S6. Superimposed DOSY ^{1}H spectra of P3HT-*b*-PMMA and two homopolymers in benzene-d6. The ^{1}H spectrum of block copolymer is shown at the top.

As shown in Figure S6, ^{1}H signals corresponding to ethynyl-P3HT, azido-PMMA, and P3HT-*b*-PMMA had different diffusion coefficients and only one diffusion coefficient was observed from P3HT-*b*-PMMA, which allowed us to conclude that one single diblock copolymer was present in the sample and free of any homopolymers.

In order to check the microstructure of the diblock copolymers SAXS and WAXS experiments were performed at different temperatures (figure S7, S8, S9, S13 and S14). Wide-angle and small-angle X-ray scattering (WAXS and SAXS) experiments were performed by using a rotating anode generator (Rigaku Nanoviewer MicroMax) and a NanoStar-Bruker AXS setup working a sample-to-detector distance of 309 and 1046 mm, respectively. Both setups produced X-ray beam with a wavelength of 1.54 Å and were equipped with a homemade heating stages having a thermal stability of 0.1°C for temperature dependence experiments.

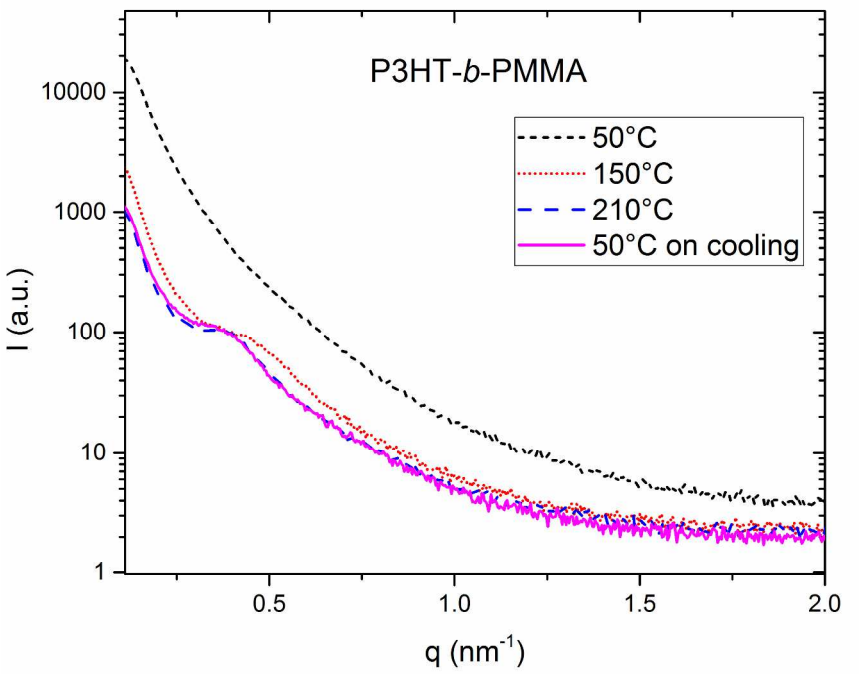

Figure S7. The SAXS spectra of **P3HT-*b*-PMMA** at different temperatures.

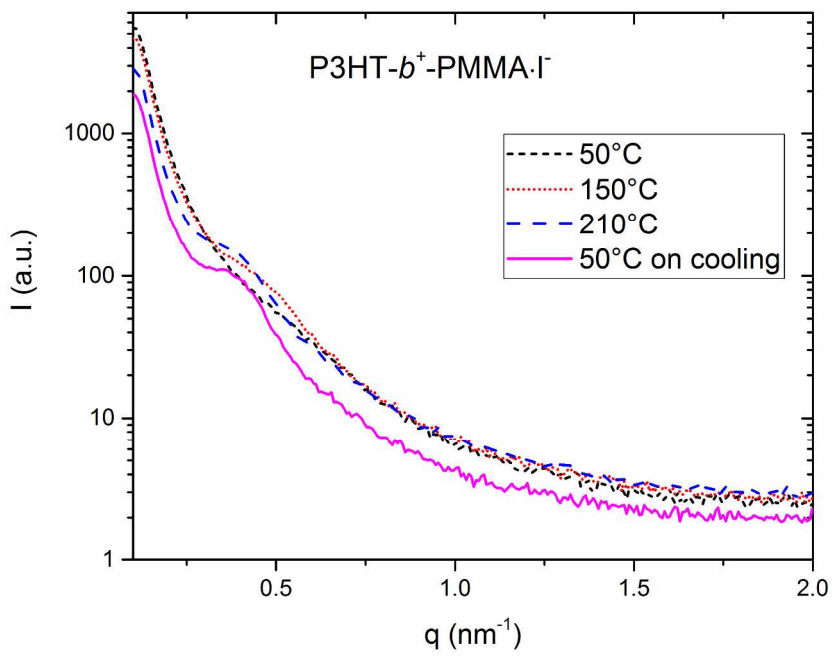

Figure S8. The SAXS spectra of **P3HT-*b*$^{+}$-PMMA I^{-}** at different temperatures.

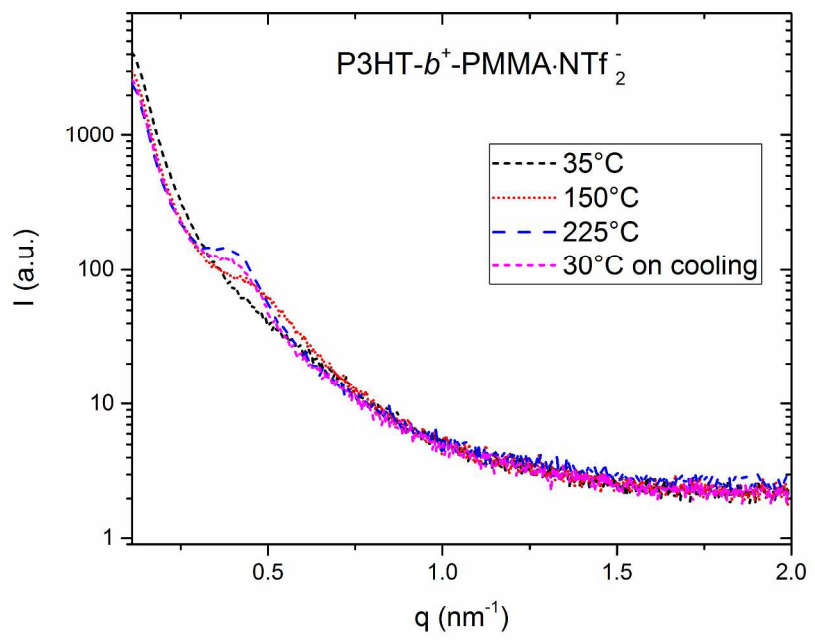

Figure S9. The SAXS spectra of **P3HT-b^+-PMMA NTf_2^-** at different temperatures.

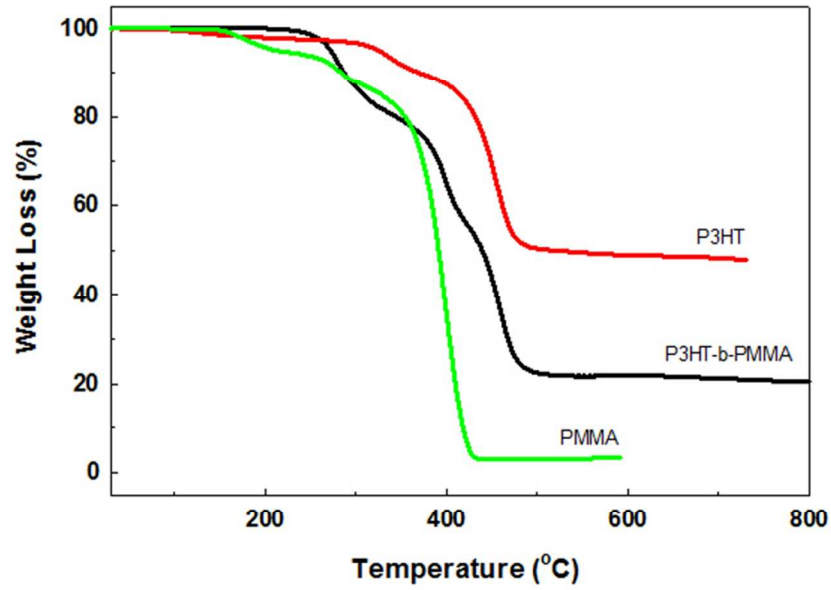

Figure S10. Thermogravimetric analysis of P3HT and PMMA homopolymer and the neutral copolymer.

Diblock samples degradation starting at around 240°C (Figure S10).

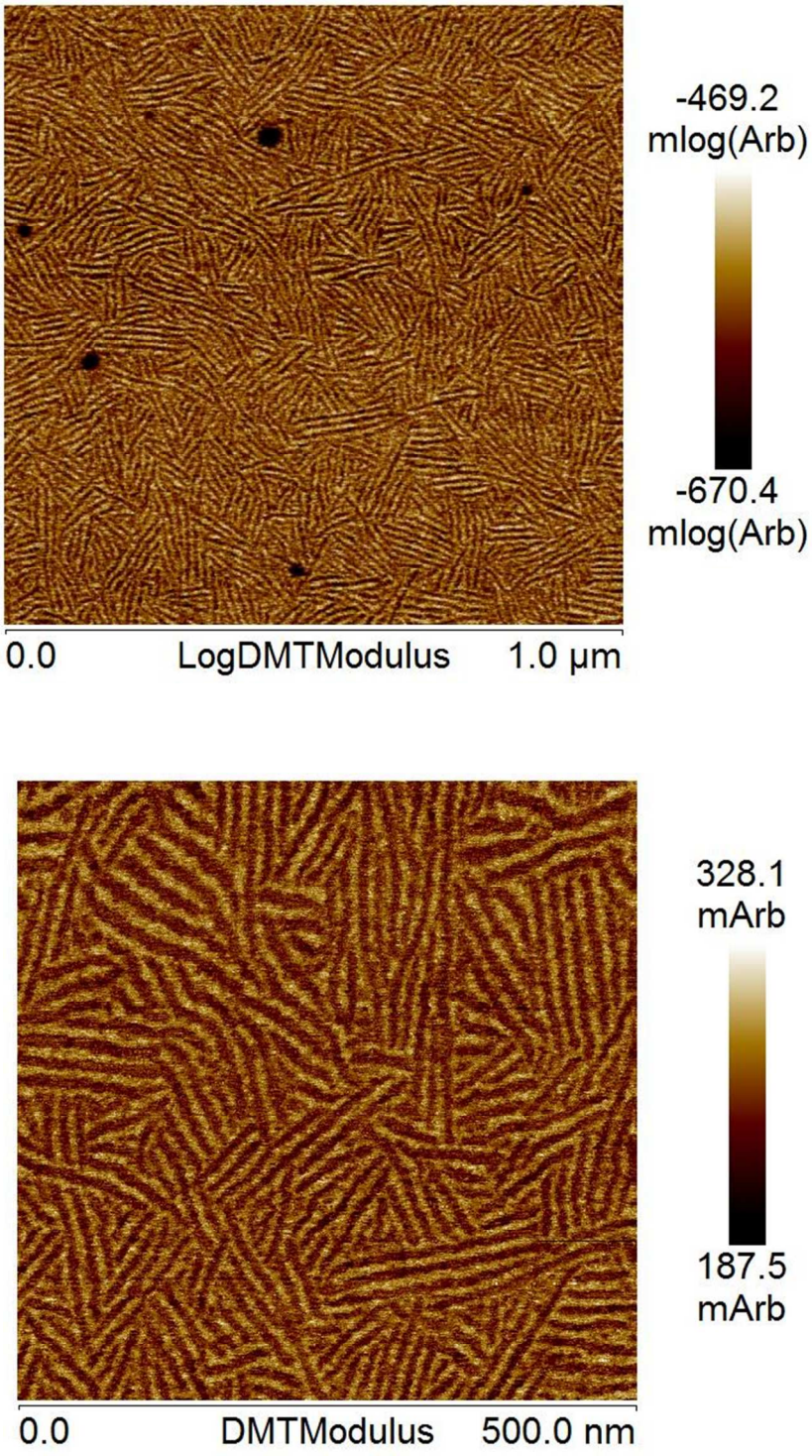

Figure S11. PeakForce QNM-mode AFM images of P3HT-b^{+}-PMMA$\cdot$ I^{-} films thermally annealed at 200 ^{o}C.

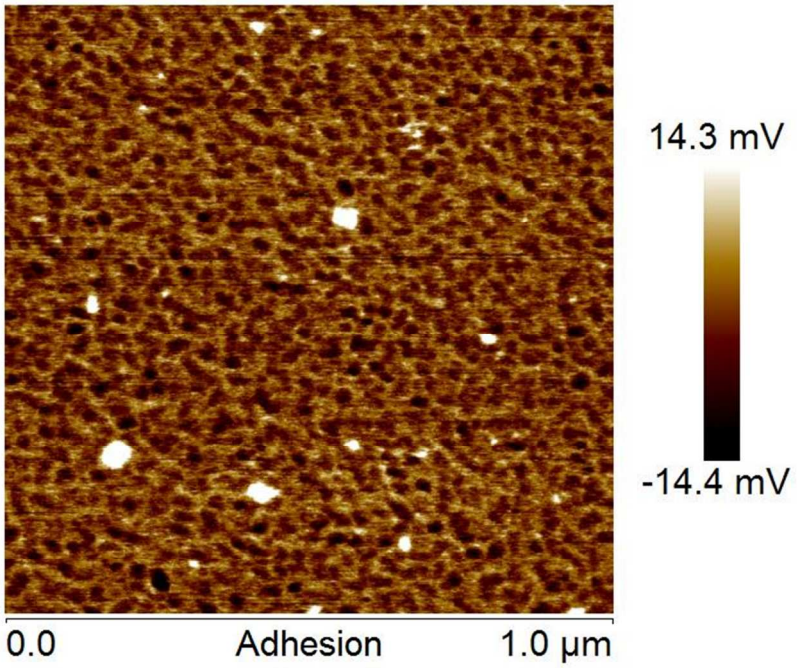

Figure S12. Adhesion-mode AFM images of P3HT-b^{+}-PMMA· NTf_2^{-} films thermally annealed at 200 ^{o}C.

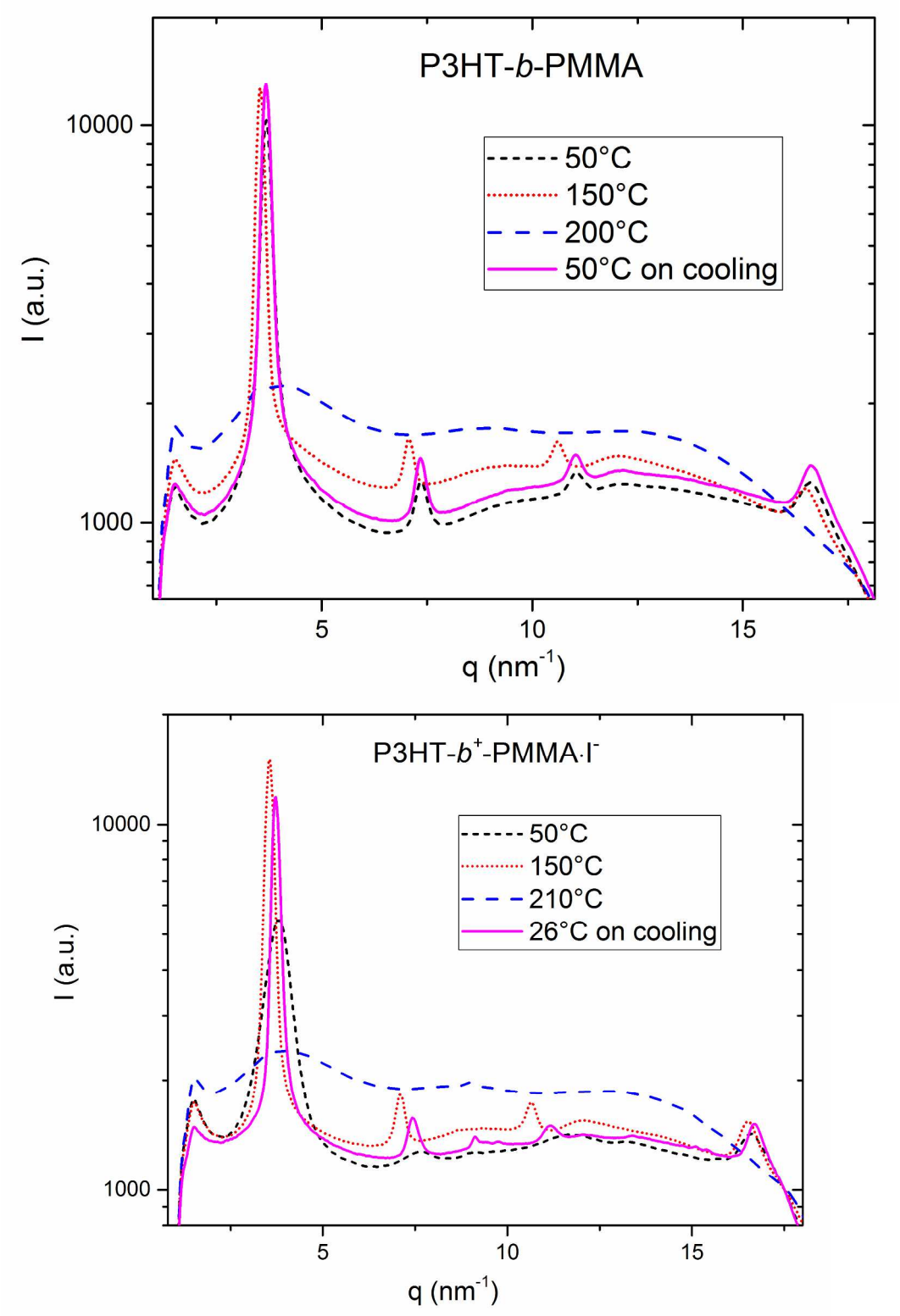

Figure S13. The WAXS spectra of **P3HT-*b*-PMMA and P3HT-b^+-PMMA I^-** at different temperatures.

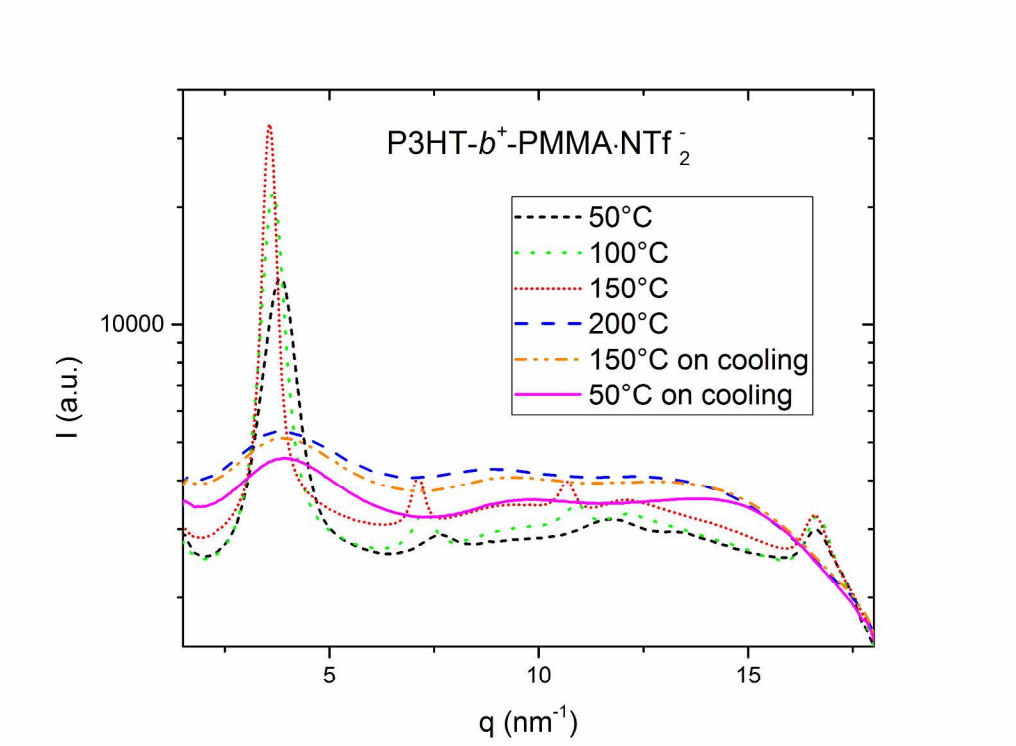

Figure S14. The WAXS spectra of **P3HT-b^+-PMMA NTf_2^-** at different temperatures.

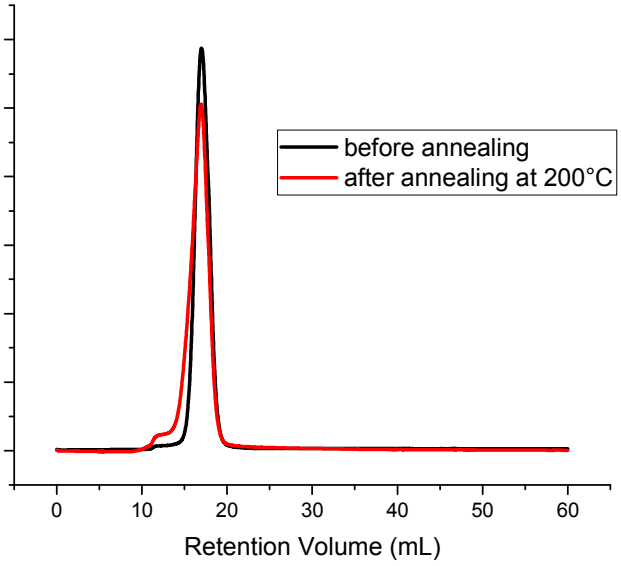

Figure S15. SEC UV-spectrum of P3HT-b^+-PMMA I^-, before and after heating at 200 °C.

Figure S15 show that after an annealing at 200°C the copolymers main chains are not thermally degraded. Thus the system is still composed of pure diblock copolymer.

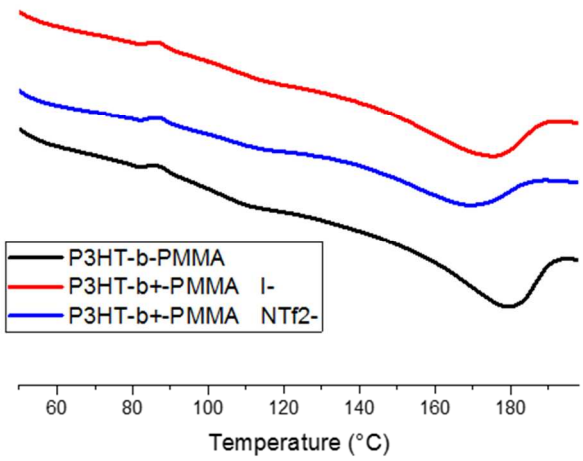

Figure S16. DSC curves of copolymers, a heating cycle from 40 to 200°C at 10°C/min erformed after a cooling cycle from 200°C to 40°C at 1°C/min.

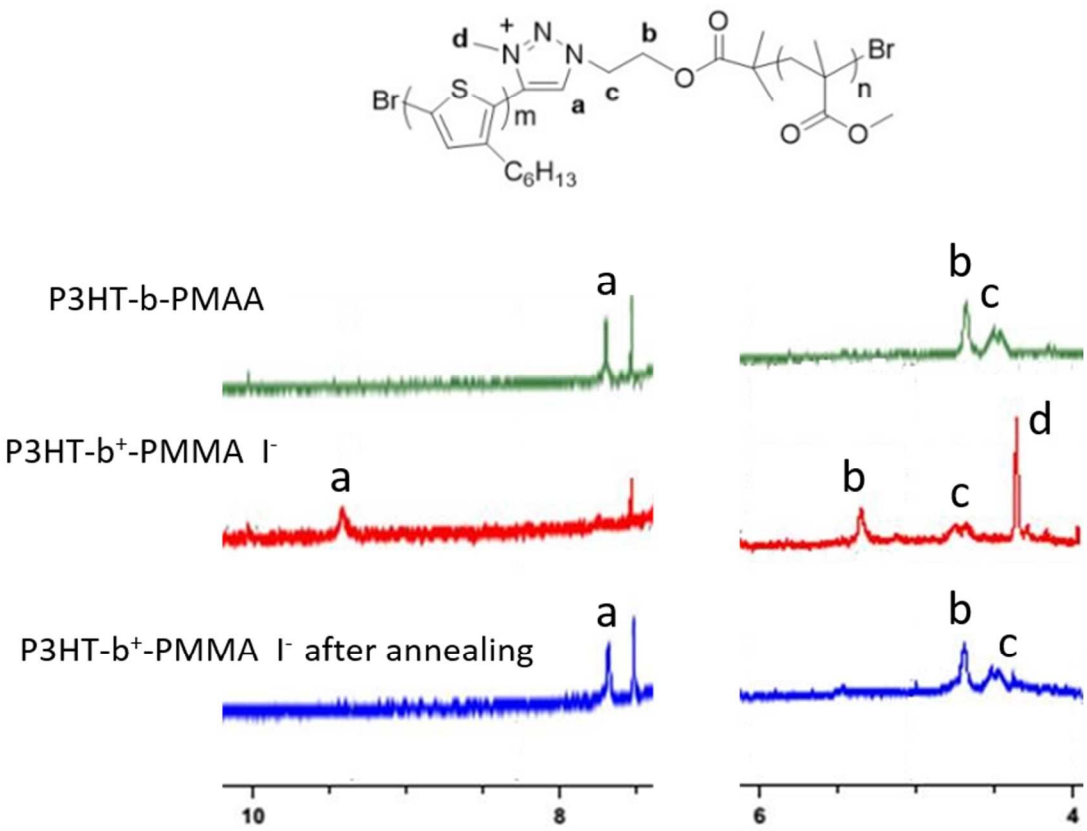

Figure S17. ^{1}H NMR spectrum of e P3HT-*b*-PMMA, P3HT-b^{+}-PMMA I^{-} and P3HT-b^{+}-PMMA I^{-} after heating at 200 C.

Figure S17 shows the degradation of the methyl iodide after an annealing of the copolymer at 200°C.